Degradation behavior at elevated temperature of $LaNi_{5-x}Sn_xH_z$ for x between 0.20 and 0.25

R.C. Bowman, Jr.[a], C.A. Lindensmith[a], S. Luo[b], Ted B. Flanagan[b], and T. Vogt[c]

[a]Jet Propulsion Laboratory, 4800 Oak Grove Dr., Pasadena, CA 91109-8099, USA,
[b]Department of Chemistry, University of Vermont, Burlington, VT 05405, USA,
[c]Department of Physics, Brookhaven National Laboratory, Upton NY 11973-5000, USA

ABSTRACT

Systematic studies of the hydriding behavior of $LaNi_{5-x}Sn_xH_z$ alloys with tin contents in the range $0.20 < x < 0.25$ have revealed changes in the pressure-composition-temperature (PCT) isotherms measured after heating the hydrides above 450 K. Some loss in reversible capacity was observed along with reductions in the plateau pressures and hysteresis ratios while the slopes of the plateau became greater. These changes are indications of degradation processes and increased disorder within the alloy structure. Additional experiments were performed for long periods (i.e., >1000 hours) at elevated temperatures and hydrogen pressure to produce further degradation in the PCT isotherms. The impact of alloy composition on the isotherms has been determined. The crystal lattice properties before and after hydrogen reactions have been studied using high-resolution x-ray powder diffraction with synchrotron radiation. Changes in these x-ray diffraction patterns are correlated to various structural modifications within the alloy induced by the hydrogen reaction.

1. Introduction

Tin (Sn) substitution for a portion of the nickel in $LaNi_5$ has been shown [1,2] to alter many of the thermodynamic properties of the resulting hydride phase as evident from the PCT isotherms for these alloys. Namely, Sn reduces the plateau pressures, hydrogen storage capacity, and hysteresis ratio while the enthalpy of formation for the hydride phase becomes more exothermic [1]. Sn levels as small as $x = 0.05$ have been found [3] to prevent formation of the intermediate γ-phase in $LaNi_5H_z$ and accompanying splitting of the plateau for $T > 350$ K. Furthermore, Sn also significantly enhances the stability of the hydride during both temperature cycling [4] under hydrogen gas and electrochemical cycling [5]. Although a complete explanation on how Sn makes the $LaNi_{5-x}Sn_xH_z$ system more robust to degradation has not been established, stronger chemical bonding of Sn to La and Ni is believed [6] to inhibit metal atom diffusion and defect/dislocation formation in the hydride. Amongst several promising applications of the Sn substituted alloys, their use in the compressors for closed-cycle, Joule-Thomson (J-T) sorption cryocoolers is especially attractive for long-life space missions [7-9]. Desirable characteristics from the sorbent hydrides in these cryocoolers include broad and flat plateaus with minimum absorption/desorption hysteresis as well as little degradation in either reversible hydrogen storage capacity or shapes of the isotherms during many thousands of cycles from 270-

300 K to 450-525 K. To satisfy the demanding performance necessary for some space missions [8,9], alloy properties need to be optimized for power efficiency, cooling temperature range and heat load, and stability during multiple year flights.

Many factors influence the hydriding properties of the AB_5 alloys, but alloy composition and stoichiometry are probably the most important. In particular, B/A ratios > 5.0 produce pressure increases, larger plateau slopes, and diminished capacities for AB_5 alloys [10,11]. The excess B atoms are accommodated in the crystal structure by B_2-dumbells randomly substituting at La sites [12]. This behavior has been previously observed for $La(Ni,Sn)_{5+x}$ alloys [13], but the impact on thermodynamic properties has not been thoroughly evaluated. The present paper reports systematic characterization of the PCT isotherms for Sn substituted alloys in the range of $0.20 < x < 0.25$ for variation of the (Ni + Sn)/La ratios from 5.00 to ~5.1 and different purity levels of the La metal. Differences were noted not only in the initial plateau pressures after activation, but also in the influence of elevated temperature (i.e., T > 450 K) on degradation induced changes in the isotherms.

2. Experimental details

The nominal $LaNi_{5-x}Sn_x$ alloys with $0.20 < x < 0.25$ were produced by either arc-melting or induction melting followed by annealing under purified argon at 1223 K for 100-120 hours as described previously [2-4]. All alloys were examined by optical metallography, powder x-ray diffraction (XRD) using Cu K_α radiation, elemental and electron microprobe analyses. Alloy compositions and crystal lattice properties are summarized in Table 1. Isotherms were measured by conventional volumetric techniques on one of two all-metal Sieverts' systems. Most isotherm data were obtained at the U. Vermont on previously described [1-3] equipment. A computer controlled apparatus utilizing an oil-free vacuum pumping station, electropolished 316L stainless steel components, and Point-of-Use filtration (MilliPore Corporation, Bedford, MA, USA) to purify further the research-grade hydrogen gas was used at the Jet Propulsion Laboratory (JPL) for isotherm determinations and long duration (> 1000 h) treatment at high temperatures (T > 460 K) and hydrogen pressure (P > 150 bar). The two systems gave indistinguishable PCT results for samples of the same alloy.

The high-resolution XRD patterns were obtained at the National Synchrotron Light Source at the Brookhaven National Laboratory as described elsewhere [13].

3. Results and Discussion

The properties for ten alloys are given in Table 1. While several alloys are nearly exactly stoichiometric (i.e., {Ni + Sn}/La = 5.00), others (i.e., samples Sn20-MPC51, Sn22-BPC872, and Sn25-MPC1860) have {Ni + Sn}/La > 5.0. There is an interesting increase in the c/a ratio from ~0.795 to 0.800 for these latter alloys which agrees with behavior of the lattice parameters for other non-stoichiometric AB_{5+x} alloys [10-13]. Although the unit cell volume increases with additional Sn substitution [14,15], the volumes are slightly smaller in Table 1 for nominally identical Sn content when {Ni + Sn}/La > 5.0. Although most alloys were found to be single phase after heat treatment at

1223 K, two (i.e., Sn25-HCI and Sn-AGR51) contained a small amount of the intermetallic LaNiSn phase [15] which reduces the proportion of Sn in the main $La(Ni,Sn)_{5+x}$ phase and thus impacts the isotherms.

Hydrogen absorption and desorption isotherms measured at 300 K for the Sn = 0.20 and 0.25 alloys and nominal Sn = 0.22 alloys are presented in Figs. 1 and 2, respectively. These results were obtained after activation [14] and completion of several isotherms at T = 373 K and lower temperatures, but no hydride formation for T > 373 K. Although it is well-established [1,14,15] that increasing the Sn content leads to cell volume expansion and decrease in plateau pressure, Fig. 1 clearly demonstrates that the pressures for the non-stoichiometric alloy Sn25-MPC1860 significantly exceeds the pressures obtained for the x = 0.20 alloy Sn20-Ref as well as the other three nearly stoichiometric Sn = 0.25 alloys. Furthermore, Sn25-MPC1860 has larger slopes across the plateau region and reduced storage capacity. These features are typical for other LaB_{5+x} alloys [10,11]. The lowest pressures and least plateau slopes among the Sn = 0.25 alloys was for the single phase Sn25-AGR50 material where presumably the Sn distribution is most uniform. In Fig. 2 the non-stoichiometric alloy Sn22-BPC872 has the highest pressures and greatest plateau slopes for the Sn = 0.22 alloys. However, the difference is not as large as seen in Fig. 1 as the deviation of the (Ni + Sn)/La ratio from 5.0 is less which is also consistent with the smaller increase in the c/a ratio for Sn22-BPC872 reported in Table 1. The results for Sn22-AGR281 in Fig. 2 also show that La metal purity impacts the isotherms mainly through reduced capacity and slightly higher pressures compared to Sn22-AGR278 made with the better La. All of the effects discussed for Figs. 1 and 2 were observed for isotherms obtained at other temperatures.

Although Sn definitely reduces disproportionation of $LaNi_{5-x}Sn_xH_z$ phases [4], some degradation at elevated temperatures has been noted. Fig. 3 shows the impact of relatively short treatments at T = 493 K and pressures above 125 bar on the post-aging 300 K isotherms for two Sn =0.22 alloys. While both systems experience downward shifts in plateau pressure and increased slopes with aging, the changes are greater for the non-stoichiometric alloy Sn22-BPC872. When hydrides of two nominally stoichiometric Sn = 0.25 alloys were aged at higher temperature and longer duration, more moderate changes were found as shown in Fig. 4. Apparently, the greater disorder in the non-stoichiometric alloys does enhance the degradation process beyond that occurring in the ideal AB_5 composition. One of the challenges is to identify the responsible mechanism.

As described by Sandrock, et al. [16], disproportionation of $LaNi_5$ hydrides can be produced by accelerated aging at high temperatures. Several samples of the Sn22-BPC872 alloy have been subjected to aging at temperatures above 460 K and pressures over 140 bar at hydride contents greater than z = 5.0. These conditions should maximize any degradation since the material should be entirely β-phase for this composition. The extent of degradation was found to increase as the aging temperature was raised. Fig. 5 shows the impact of aging at 473 K for 1,425 h on desorption isotherms at 373 K and above. Aging produced loss in reversible hydrogen storage capacity, downward shift in plateau pressure, and large increase in the slope. Similar effects were seen in absorption and desorption isotherms measured at lower temperature. The extensive degradation produced by 1,125h aging at 485K is shown in Fig. 6 to be removed by a regeneration treatment of ~15 h at 673K under dynamic vacuum.

Cerny et al. [17] recently indicated that comparisons of the unit cell parameters for a variety of hydrogen cycled and non-cycled AB_{5+x} samples often yield an **a** axis decrease while the **c** axis expands to leave the unit cell volume nearly constant. However, the one tin substituted alloy that Cerny et al. had examined (i.e., $LaNi_{4.5}Sn_{0.5}$) showed an increase of both **a** and **c**. Using high-resolution XRD, a range of different responses of the unit cell parameters upon cycling have been observed which cannot be generalized in such a simple and straightforward mechanism. They indicate that a far more complex microstructure evolves along with the changes observed in PCT-isotherms and their degradation over time.

For a Sn22-BPC872 sample which underwent just two 373 K and one 300 K H_2 cycling processes, the **a** axis decreased from 0.505291(8) nm to 0.505207(4) nm; whereas the **c** axis remains constant (i.e., 0.402894(22) nm to 0.402895(14) nm) compared to the unreacted alloy. However, a Sn22-BPC872 sample that was used for eighteen hydriding cycles at various temperatures up to T = 493 K and also exhibited the downward shift in plateau pressures shown in Fig. 3 had increases of both **a** and **c** axis to 0.505619(13) nm and 0.403229(29) nm, respectively. Williamson-Hall analyses [18] of the XRD peak widths were used to determine the mean crystallite size L and distribution of the d-spacings $\Delta d/d$ for these samples. It was found that the compositional fluctuations, which were extracted from the slopes after correcting for the instrumental contributions, remain constant after initial hydriding cycles. However, the significant line broadening of the ***00l*** reflections indicated the 'correlation length' along the c-axis decreases from ~350 nm to ~ 150 nm. For the alloy that was cycled more times and up to T = 493 K, this correlation length remains constant along with the compositional fluctuation, but there were increases for both **a** and **c** axes. This behavior could be indicative of the interplay between first- and second-type effects as discussed by Krivoglaz [19]. First-type effects such as dislocation loops, dipoles, vacancies and interstitials change the lattice parameters but result in no line broadening; whereas, second-type defects such as dislocations induce line broadening but no change of lattice parameters. It appears that both types are occurring at different stages of the hydriding process for these $La(Ni,Sn)_{5+x}$ alloys.

Comparisons of the high-resolution XRD parameters for two Sn = 0.25 alloys from Fig. 4 before and after the completion of the cycling to T > 495 K were also performed. The Sn25-AGR50 samples indicate the similar increase of the **a** and **c** unit cell parameters upon hydriding as seen for the Sn = 0.22 alloy while the slope of the Williamson-Hall plots indicates that the strain inferred from the $\Delta d/d$ variations remains constant within the errors. The Sn25-AGR51 alloys show another type of response to hydriding: this time the **a** unit cell parameter increases while the **c** parameter decreases upon hydriding. The role of the secondary phase for this latter sample is unclear and needs more study. The distinct and complex behavior of tin-substituted $La(Ni,Sn)_{5+x}$ alloys indicates that various mechanisms are probably involved at different stages of the hydriding process. More comprehensive investigations are needed to link the structural response with the changes observed in the PCT diagrams. Further work along these lines is in progress and will be reported at a later date.

4. Conclusions

Deviations in the stoichiometry of $La(Ni,Sn)_{5+x}$ alloys not only produce changes in hydrogen isotherms similar to those described for other $LaNi_5$-based hydrides [10,11] but their hydrides are also more vulnerable to the reversible degradation effects at elevated temperature. When less pure La metal is used to make the alloys, the hydrogen isotherms exhibit changes consistent with (Ni + Sn)/La > 5.0. Nevertheless, $LaNi_{5-x}Sn_xH_z$ with x = 0.20-0.25 is much more resistant to disproportionation reactions at T > 350 K than nearly all other AB_5 hydrides. Consequently, these alloys are the leading candidates for demanding applications such as use in the compressors of hydrogen sorption cryocoolers for space missions [7-9].

Acknowledgements

This research was carried out by the Jet Propulsion Laboratory, California Institute of Technology, under a contract with the National Aeronautical and Space Administration. Authors thank T. M. Riedemann and his colleagues at Ames Laboratory for preparation and chemical analyses of the alloys. J. G. Kulleck performed the powder XRD measurements at JPL.

References

1. S. Luo, W. Luo, J. D. Clewley, T. B. Flanagan, and L. A. Wade, *J. Alloys Comp.* **231** (1995) 467.
2. S. Luo, W. Luo, J. D. Clewley, T. B. Flanagan, and R. C. Bowman, Jr., *J. Alloys Comp.* **231** (1995) 473.
3. S. Luo, J. D. Clewley, T. B. Flanagan, R. C. Bowman, Jr., and J. S. Cantrell, *J. Alloys Comp.* **253-254** (1997) 261.
4. R. C. Bowman, Jr., C. H. Luo, C. C. Ahn, C. K. Witham, and B. Fultz, *J. Alloys Comp.* **217** (1995) 185.
5. B. V. Ratnakumar, C. Witham, R. C. Bowman, Jr., A. Hightower, and B. Fultz, *J. Electrochem. Soc.* **143** (1996) 2578.
6. R. V. Bugga, G. Halpert, B. Fultz, C. K. Witham, R. C. Bowman, Jr., and A. Hightower, U. S. Patent No. 5,656,388 Issued Aug. 12, 1997.
7. B. D. Freeman, E. L. Ryba, R. C. Bowman, Jr., and J. R. Phillips, *Int. J. Hydrogen Energy* **22** (1997) 1125.
8. P. Bhandari, R. C. Bowman, Jr., R. G. Chave, C. A. Lindensmith, G. Morgante, C. Paine, M. Prina, and L. A. Wade, *Astro. Lett. & Commun.* **37** (2000) 227.
9. L. A. Wade, P. Bhandari, R. C. Bowman, Jr., C. Paine, G. Morgante, C. A. Lindensmith, D. Crumb, M. Prina, R. Sugimura, and D. Rapp, *Adv. Cryogenic Eng.* **45** (In Press).
10. K. H. J. Buschow and H. H. van Mal, *J. Less-Common Met.* **29** (1972) 203.
11. S. Luo, T. B. Flanagan, and P. H. L. Notten, *J. Alloys Comp.* **239** (1996) 214.
12. W. Coene, P. H. L. Notten, F. Hakkens, R. E. F. Einerhand, and J. L. C. Daams, *Phil. Mag. A* **65** (1992) 1485.

13. T. Vogt, J. J. Reilly, J. R. Johnson, G. D. Adzic, and J. McBreen, *Electrochem. & Solid-State Lett.* **2** (1999) 111.
14. S. Luo, J. D. Clewley, T. B. Flanagan, R. C. Bowman, Jr., and L. A. Wade, *J. Alloys Comp.* **267** (1998) 171.
15. J.-M. Joubert, M. Latroche, R. Cerny, R. C. Bowman, Jr., A. Percheron-Guegan, and K. Yvon, *J. Alloys Comp.* **293-295** (1999) 124.
16. G. D. Sanrock, P. D. Goodell, E. L. Huston, and P. M. Golden, *Z. Physk. Chem. NF* **164** (1989) 1285.
17. R. Cerny, J.-M. Joubert, M. Latroche, A. Percheron-Guegan, and K. Yvon, *J. Appl. Cryst.* **33** (2000) 997.
18. G.K Williamson and W.H. Hall, *Acta Metall.* **1** (1953) 22.
19. M. A. Krivoglaz, *Theory of X-ray and Thermal Neutron Scattering by Real Crystals*, Plenum , New York, NY, 1969.

Figure Captions

Fig. 1. Hydrogen isotherms for $LaNi_{4.80}Sn_{0.20}$ and $LaNi_{4.75}Sn_{0.25}$ alloys at 300 K. Open symbols and solid lines represent absorption while filled symbols and dashed lines desorption.

Fig. 2. Hydrogen isotherms for $LaNi_{4.78}Sn_{0.22}$ alloys at 300 K. Open symbols and solid lines represent absorption while filled symbols and dashed lines desorption.

Fig. 3. Hydrogen isotherms for $LaNi_{4.78}Sn_{0.22}$ alloys at 300 K before and after aging at 493 K. Open symbols and solid lines represent absorption while filled symbols and dashed lines desorption.

Fig. 4. Hydrogen isotherms for $LaNi_{4.75}Sn_{0.25}$ alloys at 373 K before and after aging at $T > 495$ K. Open symbols and solid lines represent absorption while filled symbols and dashed lines desorption.

Fig. 5. Desorption isotherms for $LaNi_{4.78}Sn_{0.22}H_z$ alloy Sn22-BPC872 before (open symbols and solid lines) and after 1,425h at 473 K aging (filled symbols and dashed line) with pressure > 139 bar and initial $z = 5.29$.

Fig. 6. Hydrogen isotherms at 300K for $LaNi_{4.78}Sn_{0.22}H_z$ alloy Sn22-BPC872 before aging, after 1,125h aging at 485 K with pressure > 171 bar and initial $z = 5.10$, and vacuum regeneration at 673 K after aging. Open symbols and solid lines represent absorption while filled symbols and dashed lines desorption.

Table 1. Properties of $LaNi_{5-x}Sn_x$ alloys including lattice parameters (a, c) and hydrogen absorption (P_{abs})/desorption (P_{des}) pressures measured in plateau region (y = 2.0).

Sample ID	Alloy Composition	La Purity (at.%)	a (nm)	c (nm)	c/a	Volume ($nm^3\ 10^{-3}$)	Inclusions (Wt.%)	300 K P_{abs}/P_{des} (kPa)
Sn20-Ref	$LaNi_{4.80}Sn_{0.20}$	99.95	0.50516	0.40098	0.7953	88.62	None	56.2/47.9[a]
Sn20-MPC551	$LaNi_{4.96}Sn_{0.21}$	N. A.	0.50433	0.40249	0.7981	88.66	None	89.1/72.4
Sn22-BPC872	$LaNi_{4.87}Sn_{0.22}$	99.91	0.50512	0.40277	0.7974	89.01	None	61.7/56.5
Sn22-AGR278	$LaNi_{4.74}Sn_{0.22}$	99.91	0.50587	0.40230	0.7953	89.16	None	45.0/39.7
Sn22-AGR280	$LaNi_{4.77}Sn_{0.23}$	99.25	0.50577	0.40257	0.7960	89.18	None	50.7/43.6
Sn22-AGR281	$LaNi_{4.77}Sn_{0.23}$	98.07	0.50568	0.40251	0.7960	89.14	None	50.5/43.3
Sn25-HCl	$LaNi_{4.75}Sn_{0.25}$	N. A.	0.50625	0.40386	0.7945	89.27	LaNiSn (~1+ %)	40.7/32.4
Sn25-MPC1860	$LaNi_{4.91}Sn_{0.27}$	99.87	0.50439	0.40386	0.8007	88.98	None	72.4/64.6
Sn25-AGR50	$LaNi_{4.75}Sn_{0.25}$	99.80	0.50651	0.40269	0.7950	89.47	None	33.1/30.2
Sn25-AGR51	$La_{1.02}Ni_{4.75}Sn_{0.25}$	99.80	0.50629	0.40217	0.7948	89.18	LaNiSn (~2 %)	45.2/38.0

[a]Isotherm previously measured at 298 K (Ref. 2)

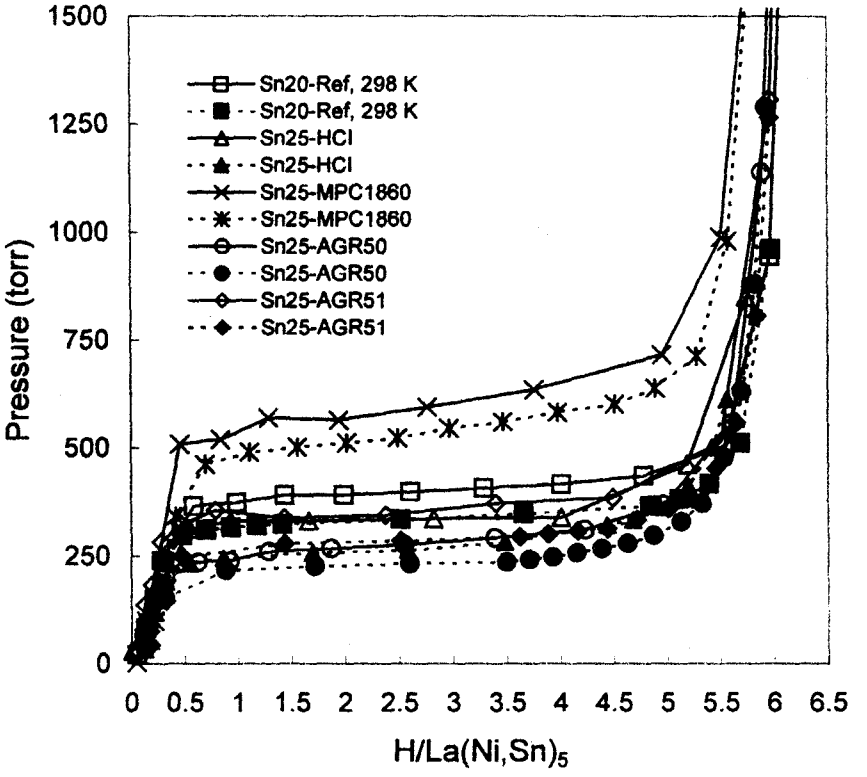

Fig. 1. Hydrogen isotherms for $LaNi_{4.80}Sn_{0.20}$ and $LaNi_{4.75}Sn_{0.25}$ alloys at 300 K. Open symbols and solid lines represent absorption while filled symbols and dashed lines desorption.

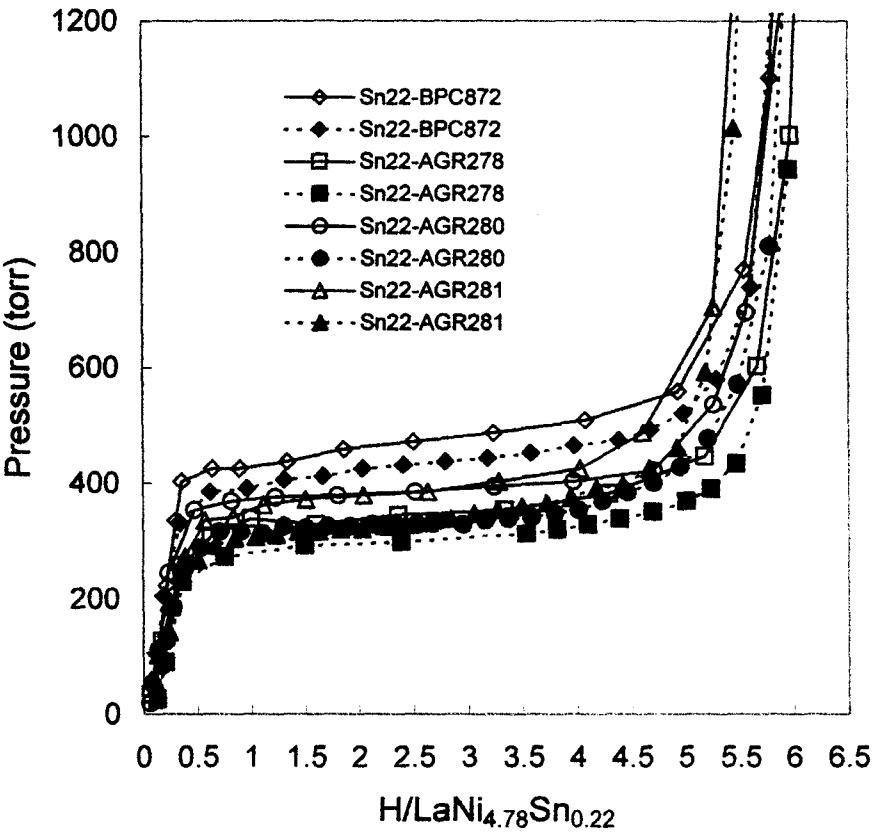

Fig. 2. Hydrogen isotherms for $LaNi_{4.78}Sn_{0.22}$ alloys at 300 K. Open symbols and solid lines represent absorption while filled symbols and dashed lines desorption.

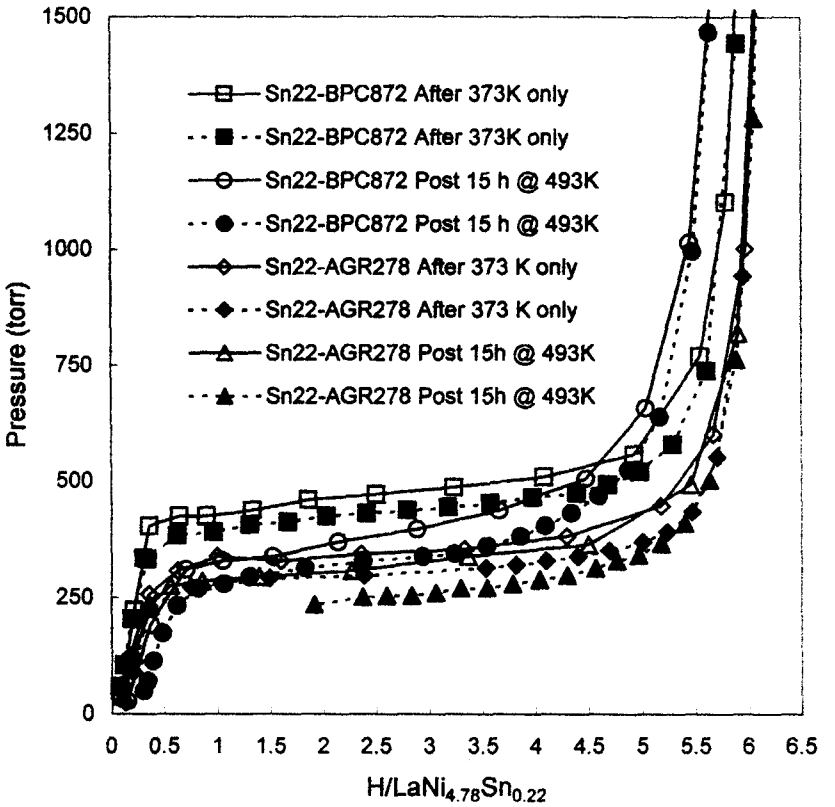

Fig. 3. Hydrogen isotherms for $LaNi_{4.78}Sn_{0.22}$ alloys at 300 K before and after aging at 493 K. Open symbols and solid lines represent absorption while filled symbols and dashed lines desorption.

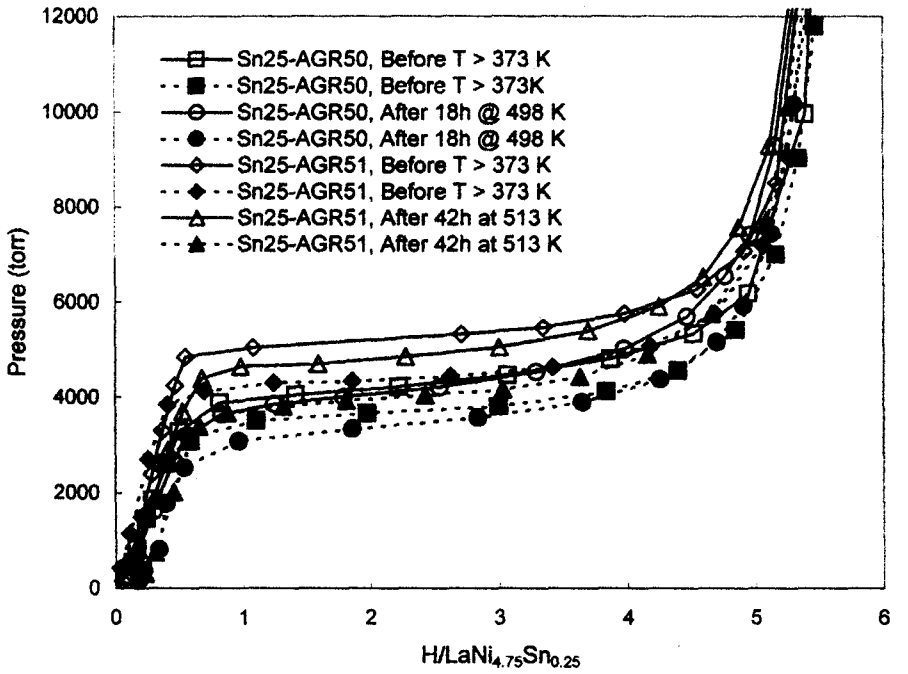

Fig. 4. Hydrogen isotherms for $LaNi_{4.75}Sn_{0.25}$ alloys at 373 K before and after aging at 493 K. Open symbols and solid lines represent absorption while filled symbols and dashed lines desorption.

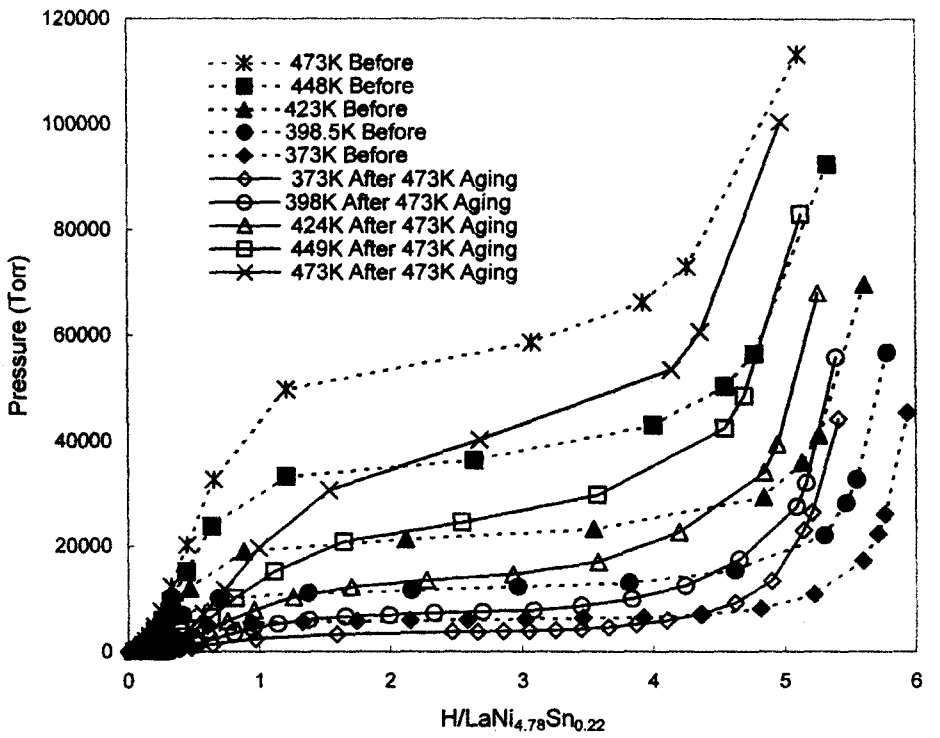

Fig. 5. Desorption isotherms for $LaNi_{4.78}Sn_{0.22}H_z$ alloy Sn22-BPC872 before (open symbols and solid lines) and after 1,425h at 473 K aging (filled symbols and dashed line) with pressure > 139 bar and initial z = 5.29.

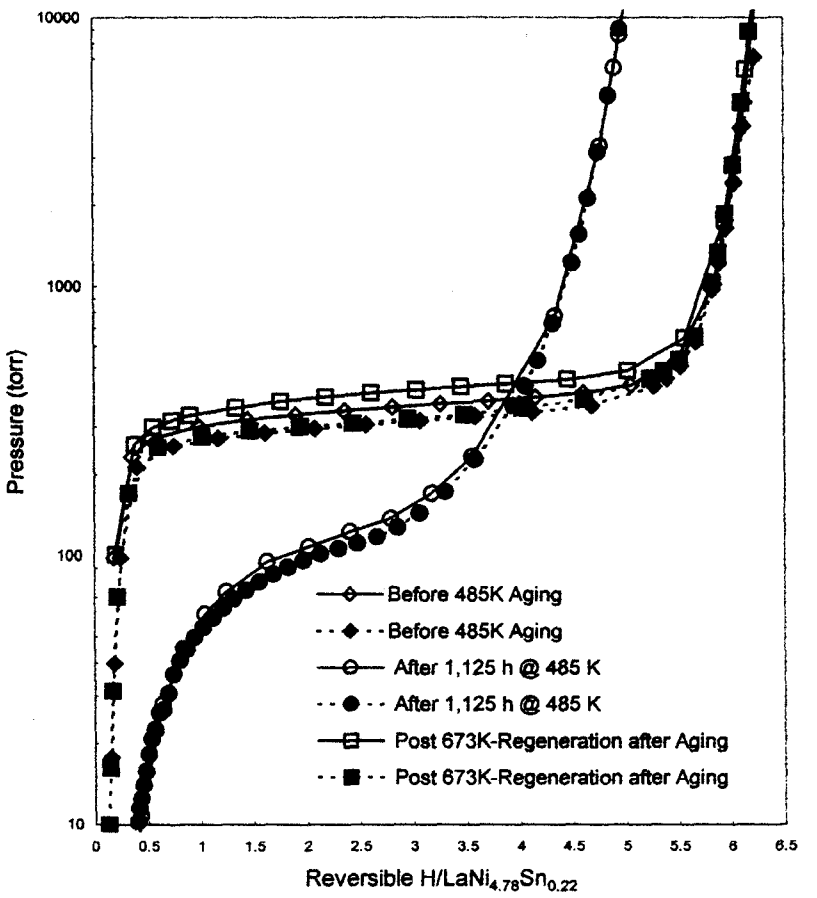

Fig. 6. Hydrogen isotherms at 300K for $LaNi_{4.78}Sn_{0.22}H_z$ alloy Sn22-BPC872 before aging, after 1,125h aging at 485 K with pressure > 171 bar and initial z = 5.10, and vacuum regeneration at 673 K after aging. Open symbols and solid lines represent absorption while filled symbols and dashed lines desorption.